

2 **Determination of muon momentum in the**  
3 **MicroBooNE LArTPC using an improved model of**  
4 **multiple Coulomb scattering**

---

5 **The MicroBooNE Collaboration**

6 ABSTRACT: We discuss a technique for measuring a charged particle's momentum by means of  
7 multiple Coulomb scattering (MCS) in the MicroBooNE liquid argon time projection chamber  
8 (LArTPC). This method does not require the full particle ionization track to be contained inside of  
9 the detector volume as other track momentum reconstruction methods do (range-based momentum  
10 reconstruction and calorimetric momentum reconstruction). We motivate use of this technique,  
11 describe a tuning of the underlying phenomenological formula, quantify its performance on fully  
12 contained beam-neutrino-induced muon tracks both in simulation and in data, and quantify its  
13 performance on exiting muon tracks in simulation. We find agreement between data and simulation  
14 for contained tracks, with a small bias in the momentum reconstruction and with resolutions that  
15 vary as a function of track length, decreasing from about 10% for the shortest (one meter long)  
16 tracks to 5% for longer (several meter) tracks. For simulated exiting muons with at least one meter  
17 of track contained, we find a similarly small bias, and a resolution which is less than 15% for muons  
18 with momentum below 2 GeV/c though higher at higher momenta.

---

19	<b>Contents</b>	
20	<b>1 Introduction and motivation</b>	1
21	<b>2 Multiple Coulomb scattering</b>	2
22	2.1 Tuning the Highland formula for argon	4
23	<b>3 MCS implementation using the maximum likelihood method</b>	6
24	3.1 Track segmentation and scattering angle computation	7
25	3.2 Maximum likelihood theory	7
26	3.3 Maximum likelihood implementation	8
27	<b>4 Range-based energy validation from simulation</b>	8
28	<b>5 MCS performance on beam neutrino-induced muons in MicroBooNE data</b>	10
29	5.1 Input sample	10
30	5.2 Event selection	10
31	5.3 Validation of the Highland formula	11
32	5.4 MCS momentum validation	11
33	5.5 Impact of Highland formula tuning	12
34	<b>6 MCS performance on exiting muons in MicroBooNE simulation</b>	15
35	<b>7 Conclusions</b>	16

---

## 36 **1 Introduction and motivation**

37 In this paper we summarize the theory of multiple Coulomb scattering (MCS) and describe how the  
38 underlying Highland formula is retuned based on Monte Carlo simulation for use in liquid-argon  
39 time-projection chambers (LArTPCs). We present a maximum likelihood based algorithm that is  
40 used to determine the momentum of particles in a LArTPC. The only way to determine the mo-  
41 mentum of a particle that exits the active volume of a LArTPC is through MCS measurements. We  
42 demonstrate that this technique works well for a sample of fully contained muons from Booster  
43 Neutrino Beam (BNB)  $\nu_\mu$  charged-current (CC) interactions, and determine the resolutions and bi-  
44 ases of the measurement. In addition we demonstrate the performance of the method on simulated  
45 exiting tracks.

46  
47 MicroBooNE (Micro Booster Neutrino Experiment) is an experiment that uses a large LArTPC  
48 to investigate the excess of low energy events observed by the MiniBooNE experiment [1] and to  
49 study neutrino-argon cross-sections. MicroBooNE is the first detector of the Short-Baseline Neu-  
50 trino (SBN) [2] physics program at the Fermi National Accelerator Laboratory (Fermilab), to be

joined by two other LArTPCs: the Short Baseline Near Detector (SBND) and the Imaging Cosmic And Rare Underground Signal (ICARUS) detector [3]. MicroBooNE also performs important research and development in terms of detector technology and event reconstruction techniques for future LArTPC experiments including DUNE (Deep Underground Neutrino Experiment) [4].

55

The MicroBooNE detector [5] consists of a rectangular time-projection chamber (TPC) with dimensions  $2.6 \text{ m} \times 2.3 \text{ m} \times 10.4 \text{ m}$  (width  $\times$  height  $\times$  length) located 470 m downstream from the Booster Neutrino Beam (BNB) target [6]. LArTPCs allow for precise three-dimensional reconstruction of particle interactions. For later reference, the  $z-$  axis of the detector is horizontal, along the direction of the BNB, while the  $x-$  direction of the TPC corresponds to the drift coordinate and the  $y-$  direction is the vertical direction. The mass of active liquid argon contained within the MicroBooNE TPC volume is 89 tons, out of a total mass of 170 tons.

63

A set of 32 photomultiplier tubes (PMTs) and three planes of wires with 3 mm spacing at angles of 0, and  $\pm 60$  degrees with respect to the vertical are located in the TPC for event reconstruction as shown in figure 1. The cathode plane operating voltage is -70 kV. A neutrino in the beam interacts with an argon nucleus and the charged outgoing particles traverse the medium, lose energy and leave an ionization trail. The resulting ionization electrons drift in a 273 V/cm electric field to the wire planes constituting the anode. The passage of these electrons through the first two wire planes induces a signal in the wires, and their collection on the third plane also generates a signal. These signals are used to create three distinct two-dimensional views (in terms of wire and time) of the event. Combining these wire signals allow for full three-dimensional reconstruction of the event, with PMT signals providing information about the absolute drift ( $x-$ ) coordinate. The boundaries of the fiducial volume used in this analysis are set back from the six faces of the active volume by distances of between 20 and 37 cm, depending on the face, to reduce the impact of electric-field non-uniformities near the edges of the TPC [7]. This volume corresponds to a mass of 55 tons.

78

The Booster Neutrino Beam (BNB) is composed predominantly of muon neutrinos ( $\nu_\mu$ ) with a peak neutrino energy of about 0.7 GeV. Some of these neutrinos undergo charge-current ( $\nu_\mu\text{CC}$ ) interactions in the TPC and produce muons and other particles. For muon tracks that are completely contained in the TPC, we calculate the momentum with a measurement of the length of the particle's track, or with calorimetric measurements which come from wire signal size measurements. Around half of the muons from BNB  $\nu_\mu\text{CC}$  interactions in MicroBooNE are not fully contained in the TPC, and therefore using a length-based or calorimetry-based method to determine the momenta for these uncontained tracks is not a possibility; the only way to determine their momenta is through MCS.

88

## 89 2 Multiple Coulomb scattering

90 Multiple Coulomb scattering occurs when a charged particle traverses medium and undergoes electromagnetic scattering off of atomic nuclei. This scattering perturbs the original trajectory of the

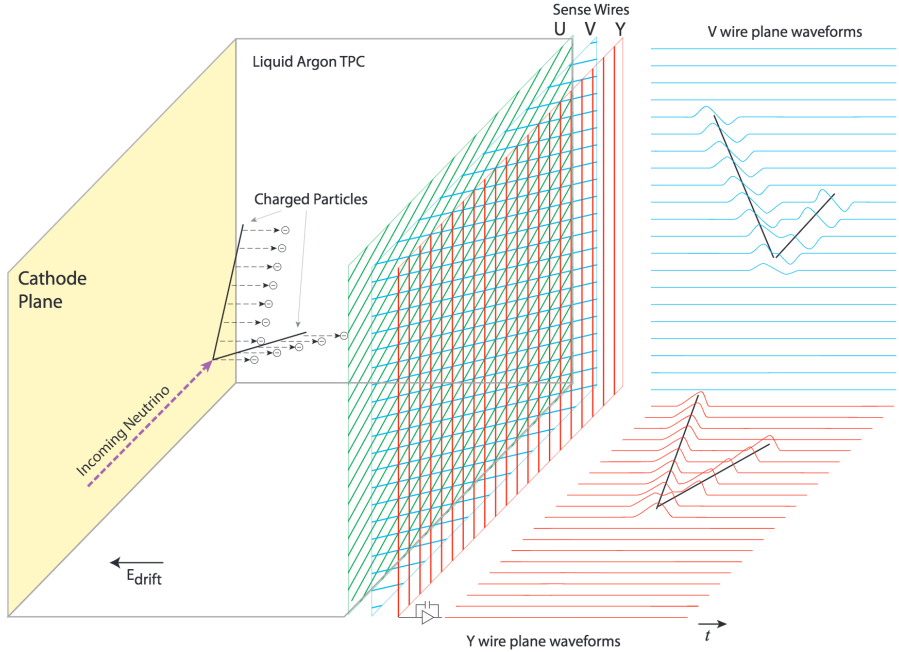


**Figure 1.** A diagram of the time projection chamber of the MicroBooNE detector [5]. PMTs (not shown) are located behind the wire planes.

92 particle within the material (figure 2). For a given initial momentum  $p$ , the angular deflection scat-  
 93 ters of a particle in either the  $x'$  direction or  $y'$  direction (as indicated in the aforementioned figure)  
 94 form a Gaussian distribution centered at zero with an RMS width,  $\sigma_o^{\text{HL}}$ , given by the Highland  
 95 formula [8][9]

$$\sigma_o^{\text{HL}} = \frac{S_2}{p\beta c} z \sqrt{\frac{\ell}{X_0}} \left[ 1 + \epsilon \times \ln\left(\frac{\ell}{X_0}\right) \right], \quad (2.1)$$

96 where  $\beta$  is the ratio of the particle's velocity to the speed of light (assuming the particle is a  
 97 muon),  $\ell$  is the distance traveled inside the material,  $z$  is the magnitude of the charge of the particle  
 98 (unity, for the case of muons), and  $X_0$  is the radiation length of the target material (taken to be a  
 99 constant 14 cm in liquid argon).  $S_2$  and  $\epsilon$  are parameters determined to be 13.6 MeV and 0.0038,  
 100 respectively. In this study, a modified version of the Highland formula is used that includes a  
 101 detector-inherent angular resolution term,  $\sigma_o^{\text{res}}$

$$\sigma_o = \sqrt{(\sigma_o^{\text{HL}})^2 + (\sigma_o^{\text{res}})^2}. \quad (2.2)$$

102 For this analysis, the  $\sigma_o^{\text{res}}$  term is given a fixed value of 3 mrad which has been determined to be  
 103 an acceptable value based on simulation studies muons at higher momenta. At 4.5 GeV/c muon  
 104 momentum and  $\ell \approx X_0$ , equation 2.1 predicts an RMS angular scatter of 3 mrad, comparable to

105 the detector resolution. The fully contained muons addressed in this analysis have momenta below  
106 1.5 GeV/c, making the impact of this detector resolution minimal for that sample.

107

108 With the Highland formula, the momentum of a track-like particle can be determined using  
109 only the 3D reconstructed track information, without any calorimetric or track range information.  
110 In neutrino physics experiments, past emulsion detectors like the DONUT [10] and OPERA [11]  
111 Collaborations have used MCS to determine particle momenta. Additionally, the MACRO [12]  
112 Collaboration at Gran Sasso Laboratory utilized this technique. The original method for using  
113 MCS to determine particle momentum in a LArTPC used a Kalman Filter and was described  
114 by the ICARUS collaboration [13], and they more recently described another method [14]. The  
115 likelihood-based method, discussed in this paper for use in the Microboone detector and described  
116 in detail in section 3, has improved on the ICARUS method by tuning the underlying phenomeno-  
117 logical formula.

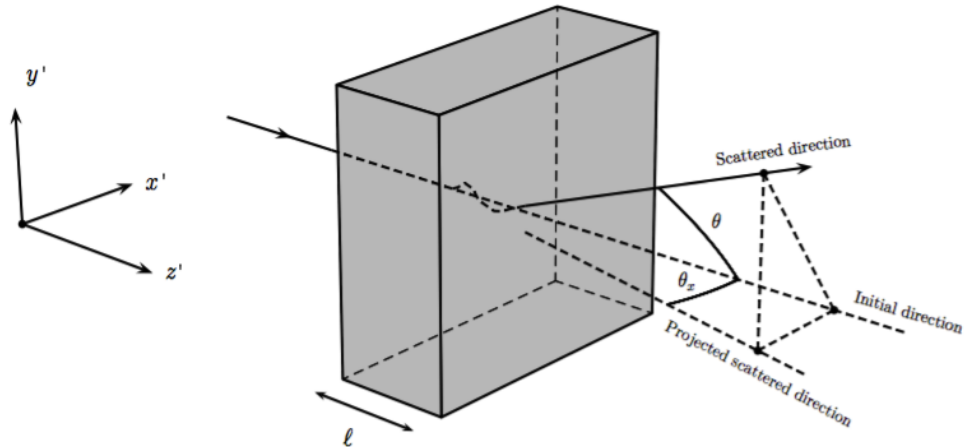


**Figure 2.** The particle’s trajectory is deflected as it traverses the material.

## 118 2.1 Tuning the Highland formula for argon

119 The Highland formula as written in equation 2.1 originates from a 1991 publication by G. R. Lynch  
120 and O. I. Dahl [9]. The parameters in the equation ( $S_2$  and  $\epsilon$ ) were determined using a global fit  
121 over MCS simulated data using a modified GEANT simulation package of 14 different elements  
122 and 7 thickness ranges. All of the simulated particles were relativistic, with  $\beta = 1$ . The materials  
123 in which they studied scattering ranged from hydrogen (with  $Z=1$ ) to uranium (with  $Z=92$ ). Given  
124 that the parameters in the formula were determined from a single fit to a wide range of  $Z$  with a  
125 wide range of material thicknesses, there is reason to believe that these parameters should differ  
126 for scattering specifically in liquid argon with  $l \approx X_0$ . There is also reason to believe that these  
127 parameters might be momentum-dependent for particles with  $\beta < 1$ , which is the case for some of  
128 the contained muons in this analysis.

129

130 In order to re-tune these parameters to liquid argon, a large sample of muons are simulated with  
 131 GEANT4 [15] in the MicroBooNE TPC and their true angular scatters are used in a fit, with  $l = X_0$ .  
 132 The reason for using  $l = X_0$  is that the Highland formula simplifies to remove its dependence on  $\epsilon$

$$\sigma_o^{\text{HL}} = \frac{S_2}{p\beta c}. \quad (2.3)$$

133 The  $S_2$  parameter in equation 2.3 is fit for as a function of true muon momentum at each scatter,  
 134 in order to explore the  $\beta$  dependence of this parameter. The fitted parameter value as a function of  
 135 true momentum is shown in figure 3.

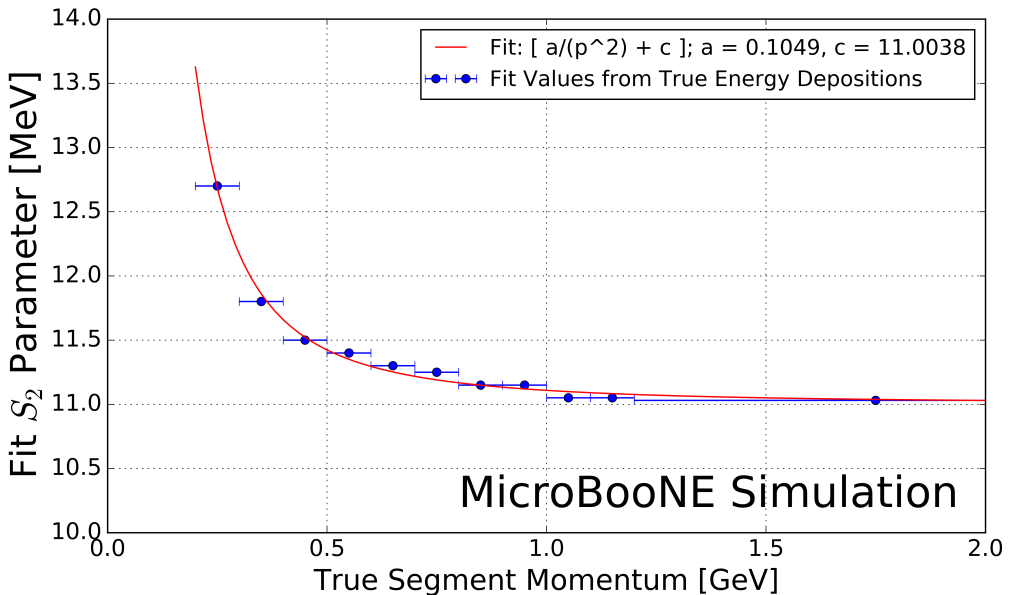


**Figure 3.** Fitted Highland parameter  $S_2$  as a function of true segment momentum for  $\ell = X_0$  simulated muons in the MicroBooNE LArTPC. Blue x- error bars indicate the true momentum bin width with data points drawn at the center of each bin. Shown in red is a fit to these data points with functional form  $a \times p^{-2} + c$ , with best fit values for parameters  $a$  and  $c$  shown in the legend.

136 The fitted value of  $S_2$  is always less than the nominal 13.6 MeV for momentum greater than  
 137 0.25 GeV/c and asymptotically approaches a constant at higher momentum (where  $\beta = 1$ ) of about  
 138 11.0 MeV. The value increases in the momentum region where  $\beta < 1$ . Shown in red is a fit to  
 139 these data points with functional form  $a \times p^{-2} + c$ , with best fit values for floating parameters  $a$   
 140 and  $c$  being  $0.105 \text{ MeV}^3 c^{-2}$  and  $11.004 \text{ MeV}$  respectively. This functional form is chosen because  
 141 it fits the data well, and asymptotically approaches a constant value when  $\beta$  approaches 1. This  
 142 function, used as a replacement for the  $S_2$  parameter in the Highland formula, will henceforth be  
 143 referred to as  $\kappa(p)$ :

$$\kappa(p) = \frac{0.105}{p^2} \text{ MeV}^3 c^{-2} + 11.004 \text{ MeV}. \quad (2.4)$$

144 To visualize the Highland formula for  $\ell = X_0$  both before and after the  $\kappa(p)$  replacement,  
 145 see figure 4. It is recommended that future LArTPC experiments use this parameterization of the

146 Highland formula, or at the very least conduct their own studies to tune the Highland formula for  
 147 scattering in argon. This formulation can also be checked in LAr-based test-beam experiments like  
 148 LArIAT [16].

149

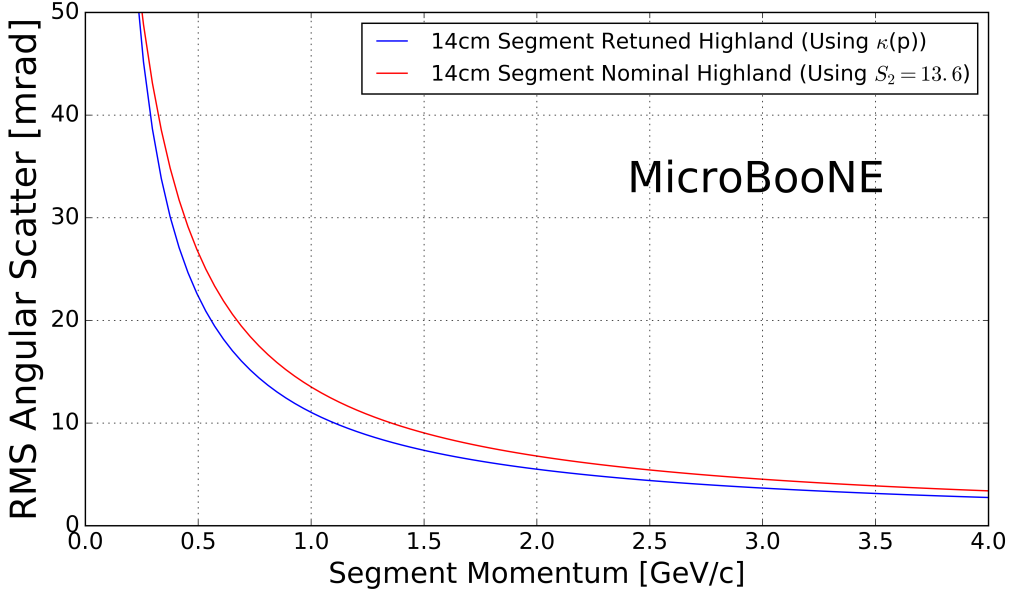


**Figure 4.** The Highland scattering RMS  $\sigma_o^{\text{HL}}$  for 14 cm segment lengths and 0 detector-inherent angular resolution as a function of true momentum before and after tuning. In red is shown equation 2.3 (the nominal Highland formula using  $S_2 = 13.6$  MeV) and in blue is the retuned Highland formula (replacing  $S_2$  with  $\kappa(p)$ ).

150 With  $\ell = X_0$ , the form of the Highland equation used in this analysis is therefore

$$\sigma_o^{\text{RMS}} = \sqrt{(\sigma_o)^2 + (\sigma_o^{\text{res}})^2} = \sqrt{\left(\frac{\kappa(p)}{p\beta c}\right)^2 + (\sigma_o^{\text{res}})^2}. \quad (2.5)$$

### 151 3 MCS implementation using the maximum likelihood method

152 This section explains in detail how the phenomenon of multiple Coulomb scattering is used to  
 153 determine the momentum of a muon track reconstructed in a LArTPC. In general, the approach is  
 154 as follows:

- 155 1. The three-dimensional track is divided into segments of configurable length.
- 156 2. The scattering angles between consecutive segments are measured.
- 157 3. Those angles combined with the modified, tuned Highland formula (equation 2.5) are used  
 158 to build a likelihood that the particle has a specific momentum, taking into account energy  
 159 loss in upstream segments of the track.

160     4. The momentum corresponding to the maximum of the likelihood is chosen to be the MCS-  
161       computed momentum.

162     Each of these steps is discussed in detail in the following subsections.

163

### 164     **3.1 Track segmentation and scattering angle computation**

165     Track segmentation refers to the subdivision of three-dimensional reconstructed trajectory points of  
166       a reconstructed track into portions of definite length. In this analysis, the tracks are automatically  
167       reconstructed by the “pandoraNuPMA” projection matching algorithm [17]. The algorithm con-  
168       structs the three-dimensional trajectory points by combining two-dimensional hits reconstructed  
169       from signals on the different wire planes along with timing information from the photomultiplier  
170       tubes. The segmentation process begins at the start of the track, and iterates through the trajectory  
171       points in order, defining segment start and stop points based on the straight-line distance between  
172       them. There is no overlap between segments. Given the subset of the three-dimensional trajectory  
173       points that corresponds to one segment of the track, a three-dimensional linear fit is applied to the  
174       data points, weighting all trajectory points equally in the fit. In this analysis, a segment length of  
175       14 cm is used, which is a tunable parameter that has been chosen as described in the derivation of  
176        $\kappa(p)$  (equation 2.4).

177

178     With the segments defined, the scattering angles between the linear fits from adjacent segments  
179       are computed. A coordinate transformation is performed such that the  $z'$  direction is oriented along  
180       the direction of the linear fit to the first of the segment pair. The  $x'$  and  $y'$  coordinates are chosen  
181       such that all of  $x'$ ,  $y'$ , and  $z'$  are mutually orthogonal and right-handed, as shown in figure 2. The  
182       scattering angles with respect to the  $x'$  direction and the  $y'$  direction are computed as input to the  
183       MCS algorithm. Only the scattering angle with respect to the  $x'$  direction is drawn in figure 2.

### 184     **3.2 Maximum likelihood theory**

185     The normal probability distribution for a scattering angle in either the  $x'$  or  $y'$  direction,  $\Delta\theta$ , with  
186       an expected Gaussian uncertainty  $\sigma_o$  and mean of zero is given by

$$f_X(\Delta\theta) = (2\pi\sigma_o^2)^{-\frac{1}{2}} \exp\left(-\frac{1}{2}\left(\frac{\Delta\theta}{\sigma_o}\right)^2\right). \quad (3.1)$$

187     Here,  $\sigma_o$  is the RMS angular deflection computed by the modified, tuned Highland formula  
188       (equation 2.5), which is a function of the momentum and the length of that segment. Since energy  
189       is lost between segments along the track,  $\sigma_o$  increases for each angular measurement along the  
190       track. We therefore replace  $\sigma_o$  with  $\sigma_{o,j}$ , where  $j$  is an index representative of the segment.

191

192     To obtain the likelihood, we take the product of  $f_X(\Delta\theta_j)$  over all  $n$  of the  $\Delta\theta_j$  segment-to-  
193       segment scatters along the track. This product can be written as

$$L(\sigma_{o,1}, \dots, \sigma_{o,n}; \Delta\theta_1, \dots, \Delta\theta_n) = (2\pi)^{-\frac{n}{2}} \times \prod_{j=1}^n (\sigma_{o,j})^{-1} \times \exp\left(-\frac{1}{2} \sum_{j=1}^n \left(\frac{\Delta\theta_j}{\sigma_{o,j}}\right)^2\right). \quad (3.2)$$

194 Rather than maximizing the likelihood it is more computationally convenient to instead min-  
 195 imize the negative log likelihood. Inverting the sign and taking  $\ln(L)$  gives an expression that is  
 196 related to a  $\chi^2$  variable:

$$-l(\mu_o; \sigma_{o,1}, \dots, \sigma_{o,n}; \Delta\theta_1, \dots, \Delta\theta_n) = -\ln(L) = \frac{n}{2} \ln(2\pi) + \sum_{j=1}^n \ln(\sigma_{o,j}) + \frac{1}{2} \sum_{j=1}^n \left(\frac{\Delta\theta_j}{\sigma_{o,j}}\right)^2 \quad (3.3)$$

### 197 3.3 Maximum likelihood implementation

198 Given a set of angular deflections in the  $x'$  and  $y'$  directions for each segment as described in  
 199 section 3.1 a scan is done over the postulated initial energy,  $E_t$ , in steps of 1 MeV up to 7.5 GeV.  
 200 The step with the smallest negative log likelihood (equation 3.3) is chosen as the MCS energy.  
 201 Equation 3.3 includes a  $\sigma_{o,j}$  term that changes for consecutive segments because their associated  
 202 energy is decreasing. The energy of the  $j$ th segment is related to  $E_t$  by

$$E_j = E_t - \Delta E_j, \quad (3.4)$$

203 where  $\Delta E_j$  is the energy loss upstream of this segment, computed by integrating the muon stopping  
 204 power curve given by the Bethe-Bloch equation described by the Particle Data Group (PDG) [19]  
 205 along the length of track upstream of this segment. Equation 3.4 introduces a minimum allowable  
 206 track energy determined by the length of the track, as  $E_j$  must remain positive. This value of  
 207 segment energy is converted to a momentum  $p$  with the relativistic energy-momentum relation  
 208 assuming the muon mass, and is then used to predict the RMS angular scatter for that segment  
 209 ( $\sigma_o$ ) by way of equation 2.5.

## 210 4 Range-based energy validation from simulation

211 In order to quantify the performance of the MCS energy estimation method on fully contained  
 212 muons in data, an independent determination of energy is needed. Range-based energy,  $E_{\text{range}}$  is  
 213 used here because the true energy  $E_{\text{true}}$  will not be known in analyzing detector data. The stopping  
 214 power of muons in liquid argon is well described by the continuous slowing-down approximation  
 215 (CSDA) by the particle data group, and agrees with data at the sub-percent level [18] [20] [21].  
 216 By using a linear interpolation between points in the stopping power table of ref. [20], the length  
 217 of a track can be used to reconstruct the muon's total energy with good accuracy. A simulated  
 218 sample of fully contained BNB neutrino-induced muons longer than one meter is used to quantify  
 219 the bias and resolution for the range-based energy estimation technique. The range is defined as the  
 220 straight-line distance between the true starting point and true stopping point of a muon, even though  
 221 the trajectories are not perfectly straight lines. The bias and resolution are computed in bins of true  
 222 total energy of the muons by fitting a Gaussian function to a distribution of the fractional energy  
 223 difference  $(E_{\text{Range}} - E_{\text{True}})/(E_{\text{True}})$  in each bin. The mean of each Gaussian yields the bias for  
 224 that true energy bin, and the width indicates the resolution. Figure 5 shows the bias and resolution for  
 225 this method of energy reconstruction increases slightly with true muon energy but remains on the  
 226 order of (2-4)%. This result demonstrates that range-based energy (and therefore range-based

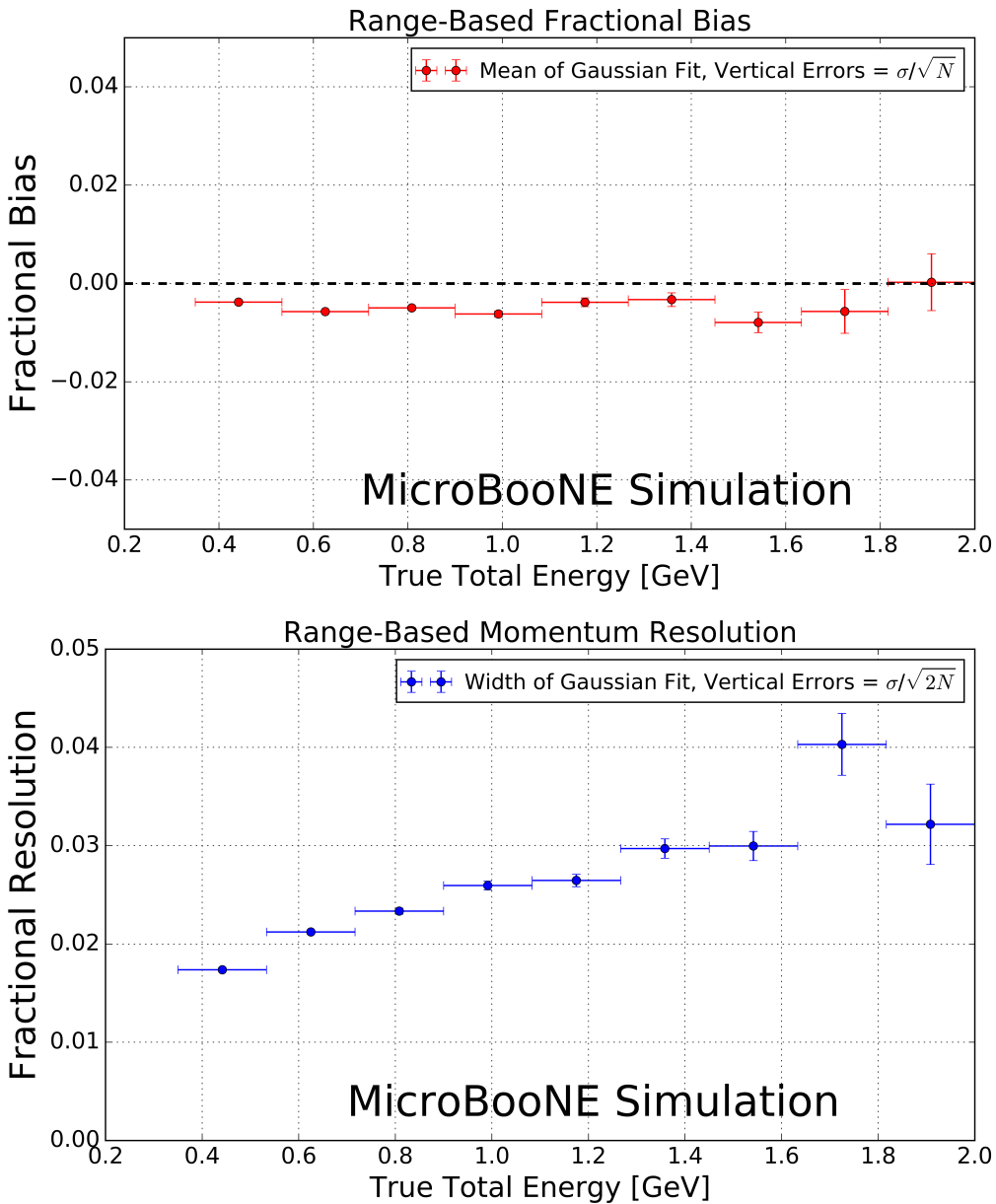


**Figure 5.** Range-based energy fractional bias (a) and resolution (b) from a sample of simulated fully contained BNB neutrino-induced muons using true starting and stopping positions of the track. The bias is less than 1% and the resolution is below  $\approx 4\%$ .

228 momentum) is a good estimator of the true energy (momentum) of a reconstructed contained muon  
 229 track in data, assuming that the track is well reconstructed in terms of length.

230 **5 MCS performance on beam neutrino-induced muons in MicroBooNE data**

231 **5.1 Input sample**

232 This part of the analysis is based on triggered neutrino interaction events in MicroBooNE corre-  
233 sponding to  $\approx 5 \times 10^{19}$  protons on target, which is a small subset (<10%) of the nominal protons  
234 on target scheduled to be delivered to the detector. These events are run through a fully automated  
235 reconstruction chain that produces reconstructed objects including three-dimensional neutrino in-  
236 teraction points (vertices), three-dimensional tracks (as described in section 3.1) for each outgoing  
237 secondary particle from the interaction, and PMT-reconstructed optical flashes from the interaction  
238 scintillation light. The fiducial volume used in this analysis is defined in section 1.

239 **5.2 Event selection**

240 The following selection criteria are placed on the reconstructed objects to select  $\nu_\mu$  charged-current  
241 interactions in which a candidate muon track exiting the interaction vertex is fully contained within  
242 the fiducial volume:

- 243 1. The event must have at least one bright optical flash, reconstructed from PMT timing signals,  
244 in coincidence with the expected BNB-neutrino arrival time.
- 245 2. Two or more reconstructed tracks must originate from the same reconstructed vertex within  
246 the fiducial volume.
- 247 3. The  $z$  coordinate of the optical flash, as determined by the pulse height and timing of signals  
248 in the 32 PMTs, must be within 70 cm of any point on the  $z$  projection of the candidate muon  
249 track.
- 250 4. For events with exactly two tracks originating from the vertex, additional calorimetric criteria  
251 are applied to mitigate backgrounds from cosmic muons that arrive in time with the passage  
252 of the beam, then stop and decay to an electron that is reconstructed as a track.
- 253 5. The longest track originating from the vertex is assumed to be a muon, and it must be fully  
254 contained within the fiducial volume.
- 255 6. The length of the longest track must be  $> 1$  m in order to have sufficient sampling points in  
256 the MCS likelihood to obtain a reasonable estimate of momentum.

257 These selection criteria are chosen to select a sample of tracks with high purity. In this sample  
258 of MicroBooNE data, 598 events (tracks) remain after all selections. The low statistics in this  
259 sample is due to the size of the input sample, described in section 5.1. Each of these events (tracks)  
260 was scanned by hand with a 2D interactive event display showing the raw wire signals of the  
261 interaction from each wire plane, with the 2D projection of the reconstructed muon track and vertex  
262 overlaid. The scanning was done to ensure the track is well reconstructed with start point close to  
263 the reconstructed vertex and end point close to the end of the visible wire-signal track in all three  
264 planes. During the scanning, obvious mis-identification topologies were removed. An example of  
265 such a topology is a stopping cosmic-ray muon decaying into an electron. After rejecting events  
266 (tracks) based on hand scanning, 396 tracks remain for analysis.

267 **5.3 Validation of the Highland formula**

268 The Highland formula indicates that distributions of angular deviations of the track, segment by  
 269 segment, in both the  $x'$  and  $y'$  directions divided by the width predicted from the Highland equation  
 270  $\sigma_o^{\text{RMS}}$  (equation 2.5) should be Gaussian with a width of unity. In order to calculate the momentum  
 271  $p$  in the Highland equation,  $p$  for each segment is computed with equation 3.4, where  $E_t$  comes  
 272 from the converged MCS-computed momentum of the track. For each consecutive pair of segments  
 273 in this sample of 396 tracks, the angular scatter divided by the Highland expected RMS (including  
 274 detector resolution term,  $\sigma_o^{\text{res}}$ ) is an entry in the area-normalized distribution shown in figure 6.  
 275 These 396 tracks have on average 12 segments each, therefore this histogram has approximately  
 276  $396 \times 12 \times 2 = 9504$  entries. The additional factor of 2 comes from angular scatters both in the  $x'$   
 277 and  $y'$  directions. The distribution has an RMS of unity, thus validating the MCS technique used  
 278 in this analysis.

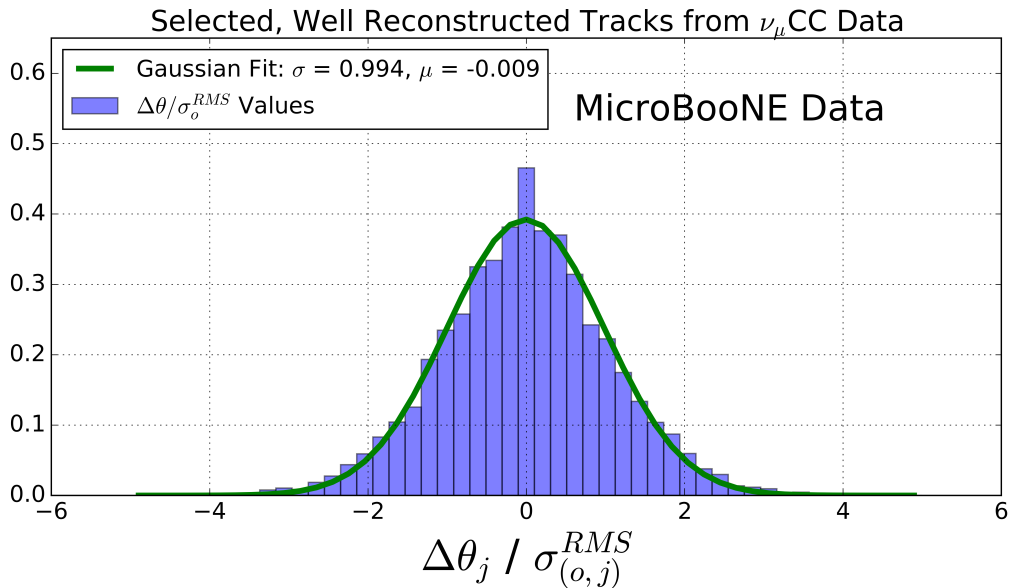


**Figure 6.** Segment-to-segment measured angular scatters in both the  $x'$  and  $y'$  directions divided by the width  $\sigma_o^{\text{RMS}}$  predicted by the Highland formula (equation 2.1) for the automatically selected beam neutrino-induced fully contained muon sample in MicroBooNE data after hand scanning to remove poorly reconstructed tracks and obvious mis-identification topologies.

279 **5.4 MCS momentum validation**

280 MCS momentum versus range-based momentum for this sample of 396 tracks is shown in figure  
 281 7. The fractional bias and resolution as a function of range-based momentum for this sample is  
 282 shown in figure 8. In order to compute this bias and resolution, distributions of fractional inverse  
 283 momentum difference  $(p_{\text{MCS}}^{-1} - p_{\text{Range}}^{-1})/(p_{\text{Range}}^{-1})$  in bins of range-based momentum  $p_{\text{Range}}$  are fit  
 284 to Gaussian functions, where the mean of the fit determines the bias while the width of the fit  
 285 determines the resolution for that bin. Inverse momentum is used here because the binned dis-  
 286 tributions are more Gaussian since the Highland formula measures inverse momentum in terms

287 of track angles that have reasonably Gaussian errors. Simply using the mean and RMS of the  
 288 binned distributions yields similar results. Also shown in this figure are the bias and resolutions  
 289 for a simulated sample consisting of a full BNB simulation with CORSIKA-generated [22] cosmic  
 290 overlays passed through an identical reconstruction and event selection chain. Rather than hand  
 291 scanning this sample, true simulation information is used by requiring the longest reconstructed  
 292 track to be matched well to the true starting and stopping point of the  $\nu_\mu$ CC muon. This removes  
 293 any mis-identifications or interference from the simulated cosmics.

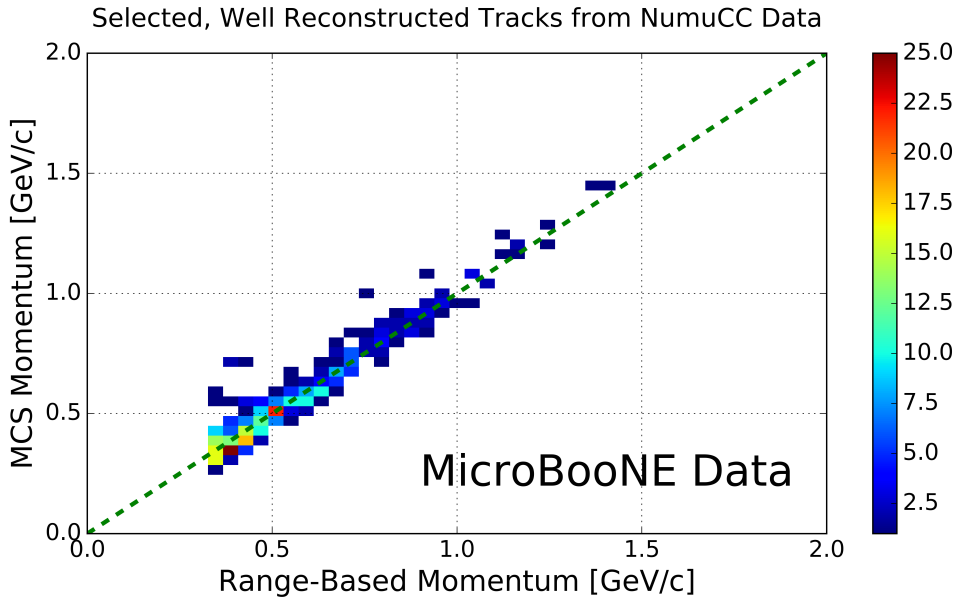


**Figure 7.** MCS-computed momentum versus range momentum for the automatically selected beam neutrino-induced fully contained muon sample in MicroBooNE data after hand scanning to remove poorly reconstructed tracks and obvious mis-identification topologies. The color (z) scale indicates number of tracks.

294 Figure 8 indicates a bias in the MCS momentum calculation on the order of a few percent, with  
 295 a resolution that decreases from about 10% for contained reconstructed tracks in data and simula-  
 296 tion with range momentum around 0.45 GeV/c (which corresponds to a length of about 1.5 m) to  
 297 below 5% for contained reconstructed tracks in data and simulation with range momentum about  
 298 1.15 GeV/c (which corresponds to a length of about 4.6 meters). Resolution improving with length  
 299 of track is intuitive; the longer the track, the more angular scattering measurements can be made  
 300 to improve the likelihood. In general the bias and resolutions agree between data and simulation  
 301 within uncertainty.

302

### 303 5.5 Impact of Highland formula tuning

304 In order to examine the impact of the Highland formula tuning described in section 2.1, the frac-  
 305 tional bias and resolution on the simulated sample of contained muons described in section 5.4 both  
 306 with the nominal Highland formula (equation 2.2) and with the retuned Highland formula (equation

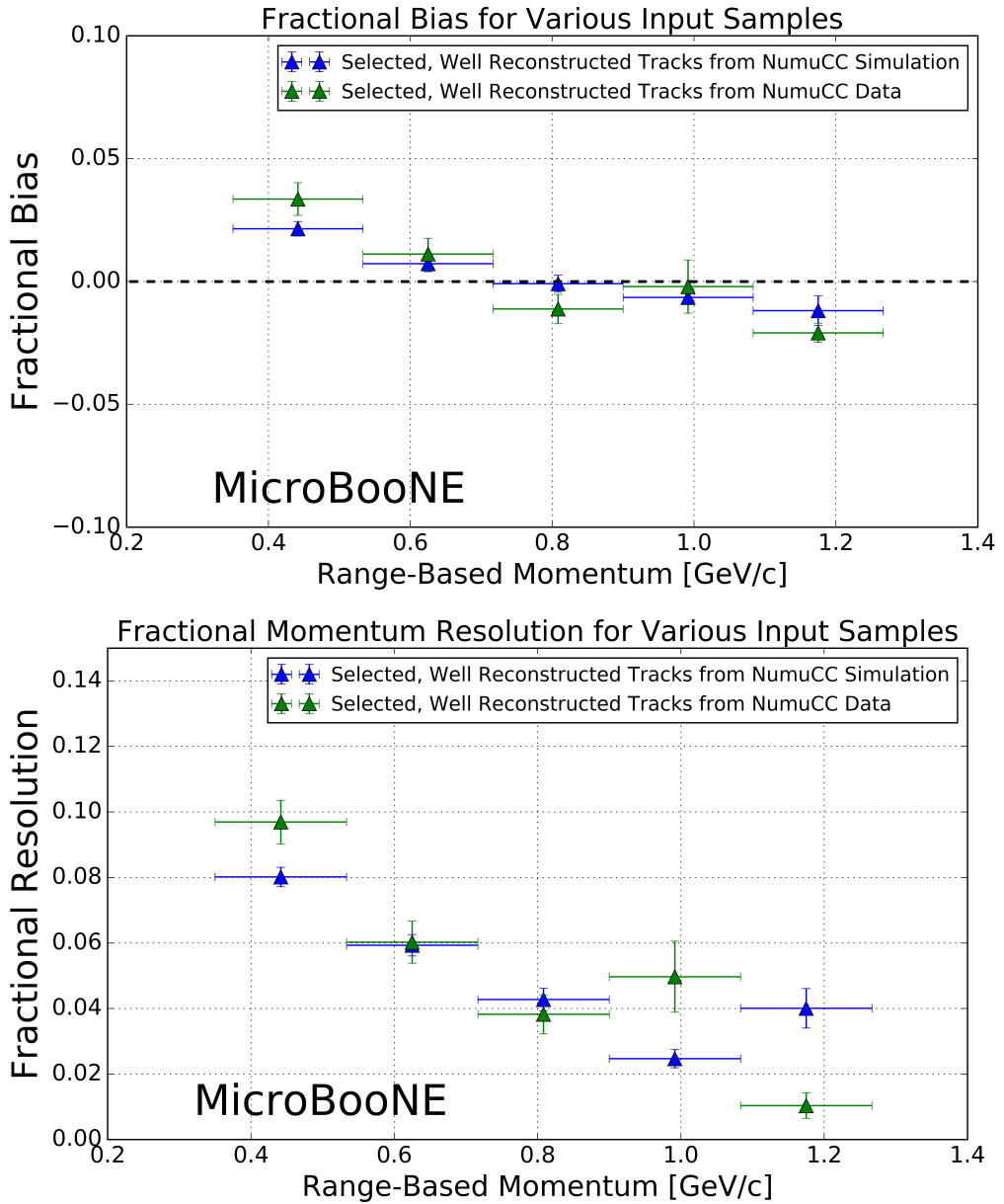


**Figure 8.** Inverse momentum difference (as defined in the text) fractional bias (top) and resolution (bottom) for automatically selected contained  $\nu_\mu$ CC-induced muons from full simulated BNB events with cosmic overlay where the track matches with the true muon track (blue), and automatically selected (see text) contained  $\nu_\mu$ CC-induced muons from MicroBooNE data (green).

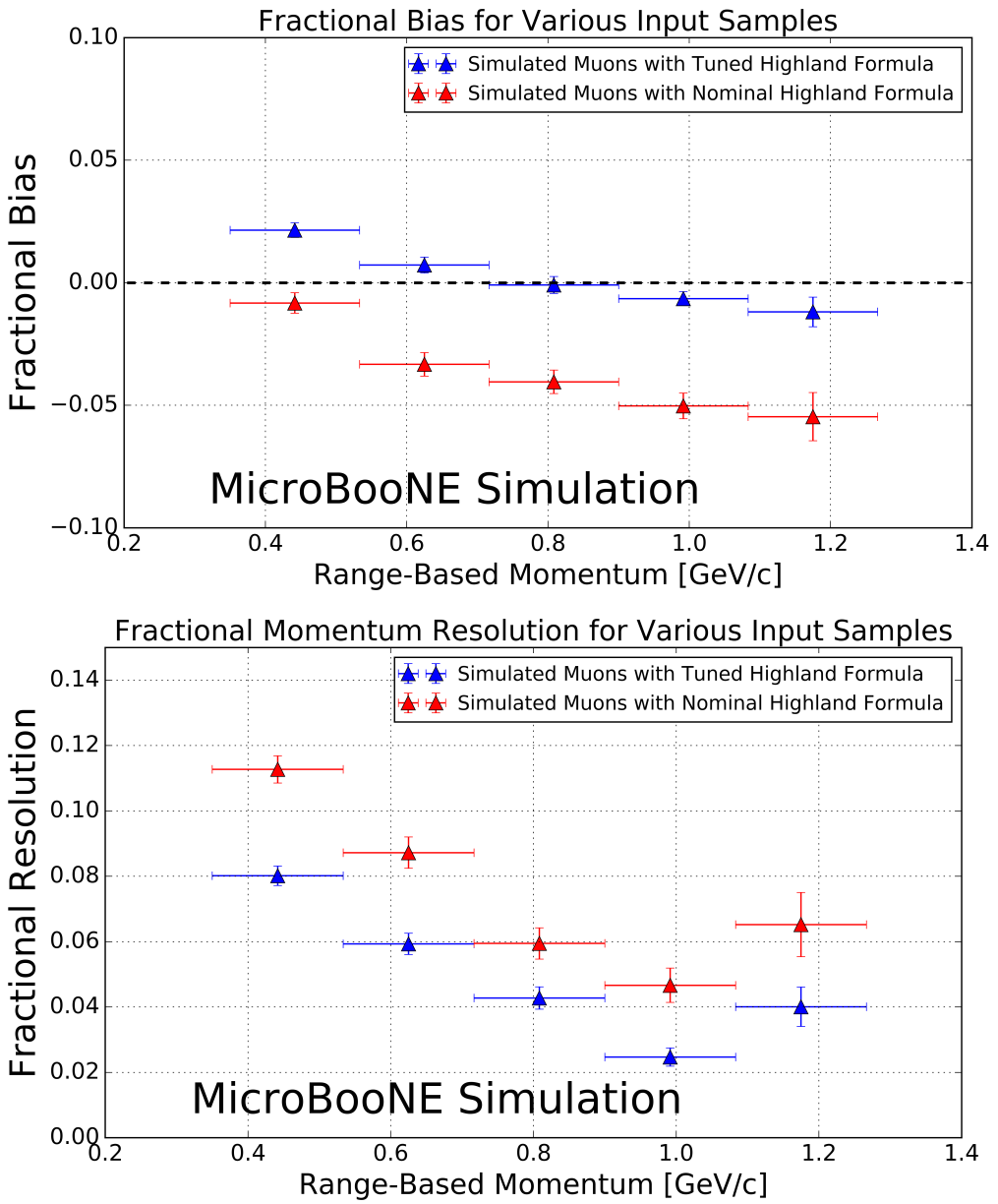


**Figure 9.** Inverse momentum difference (as defined in the text) fractional bias (top) and resolution (bottom) for automatically selected contained  $\nu_\mu$ CC-induced muons from full simulated BNB events with cosmic overlay where the track matches with the true muon track both using the nominal Highland formula (equation 2.2) (red) and the retuned Highland formula (equation 2.5) (blue).

307 2.5) are shown in figure 9. Tuning the Highland formula improves the magnitude of the fractional  
 308 bias to below 2%, and improves the fractional resolution by (2-3)% , with the most improvement at  
 309 the lowest momenta.

310 **6 MCS performance on exiting muons in MicroBooNE simulation**

311 In this section we quantify the MCS algorithm performance on a sample of exiting muon tracks in  
 312 simulated BNB  $\nu_\mu$ CC interactions within the MicroBooNE detector. The tracks are automatically  
 313 reconstructed by the same “pandoraNuPMA” algorithm described in section 3.1, and all tracks have  
 314 a length of at least 1 m within the TPC. This simulation does not include space-charge effects. The  
 315 relationship between the MCS and the true momenta at the beginning of the track as given by sim-  
 316 ulation for this sample of 28,000 exiting muon tracks is shown in figure 10.

317

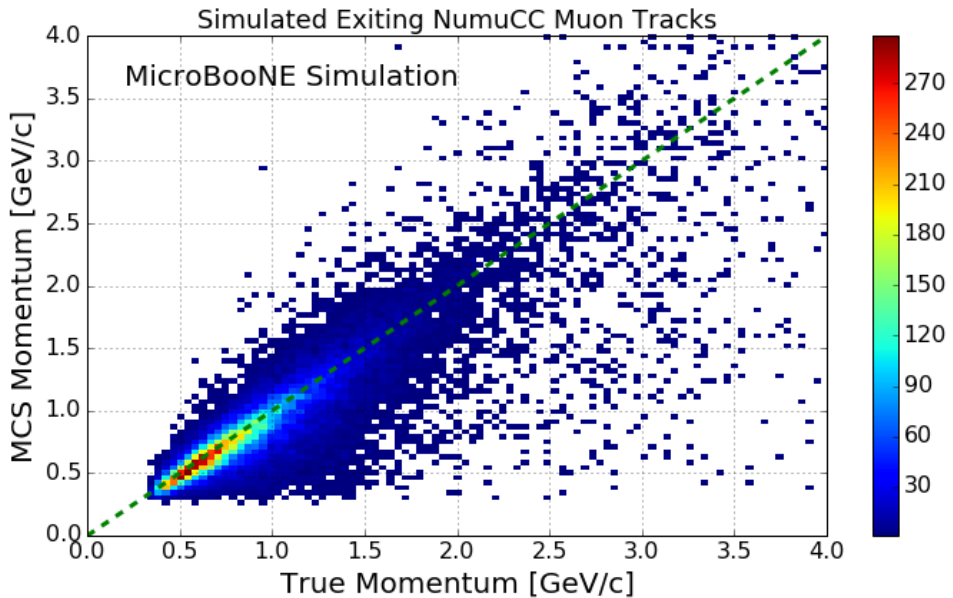


**Figure 10.** MCS-computed momentum versus true momentum for the sample of simulated exiting BNB  $\nu_\mu$ CC muons in MicroBooNE with at least one meter of track contained within the TPC. The color (z) scale indicates number of tracks.

318 The distribution of  $(p_{\text{MCS}}^{-1} - p_{\text{true}}^{-1})/(p_{\text{true}}^{-1})$  is shown for four representative bins of true momen-  
 319 tum in figure 11, along with the Gaussian fit to each distribution. Low-momentum tails where the  
 320 MCS momentum is underestimated due to poor track reconstruction lie outside the fitted Gaussian  
 321 function.

322

323 The fractional bias and resolution as a function of true momentum are shown in figure 12. The  
 324 bias is below 4% for all momenta, and the resolution is  $\approx 14\%$  in the relevant momentum region for  
 325 BNB  $\nu_\mu$ CC muons (below 2 GeV/c). The resolution worsens for muon momenta above this region  
 326 because the angular scatters begin to be comparable with the detector resolution term of 3 mrad.  
 327 The resolution improves for longer lengths of track contained, with 10% resolution for muons with  
 328  $p < 2$  GeV/c with more than 3.5 meters contained. The mean length of track contained for muons  
 329 in this analysis is 212 cm.

330

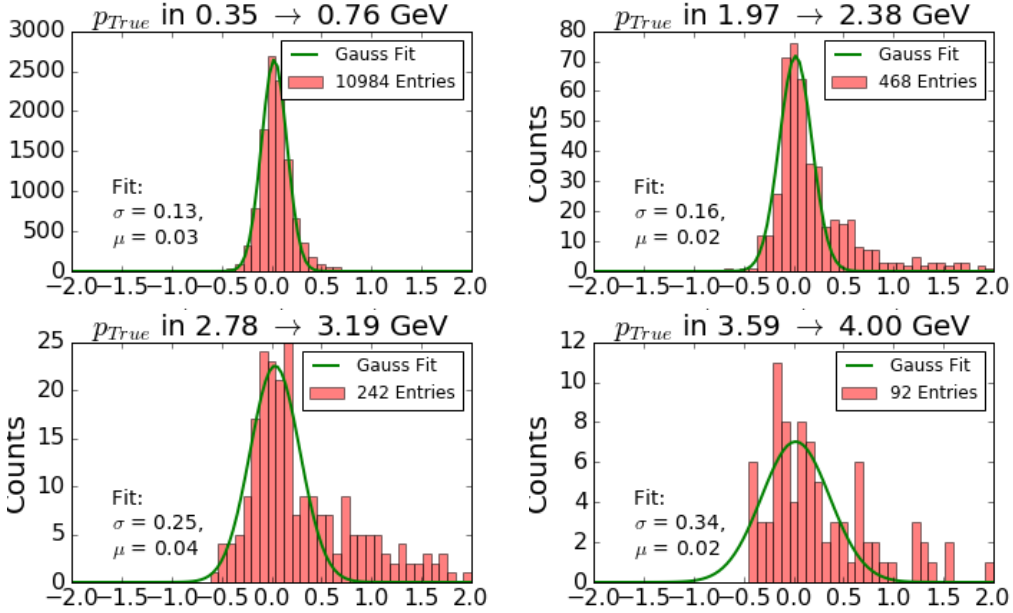


**Figure 11.** Fractional momentum difference for a few representative bins of true momentum.

## 331 7 Conclusions

332 We have described a multiple Coulomb scattering maximum likelihood method for estimating the  
 333 momentum of a three dimensional reconstructed track in a LArTPC and have provided motivation  
 334 for development of such a technique. Using simulation, we have shown that the standard Highland  
 335 formula should be re-tuned specifically for scattering in liquid argon. After validating range-based  
 336 momentum-determination techniques with MicroBooNE simulation, we have demonstrated the ac-  
 337 curacy and precision of the MCS-based momentum reconstruction in MicroBooNE data by com-  
 338 paring its performance to the range-based method. For 398 fully-contained BNB  $\nu_\mu$ CC-induced  
 339 muons, the MCS method exhibits a fractional bias below 3% and a momentum resolution below  
 340 10%, agreeing with simulation predictions. Using simulation of a separate sample of uncontained  
 341 muon tracks in MicroBooNE with at least one meter contained in the active volume, the MCS-  
 342 based reconstruction is shown to produce a fractional bias below 4% and a momentum resolution  
 343 of better than 15% for muons in the relevant BNB energy region of below 2 GeV.

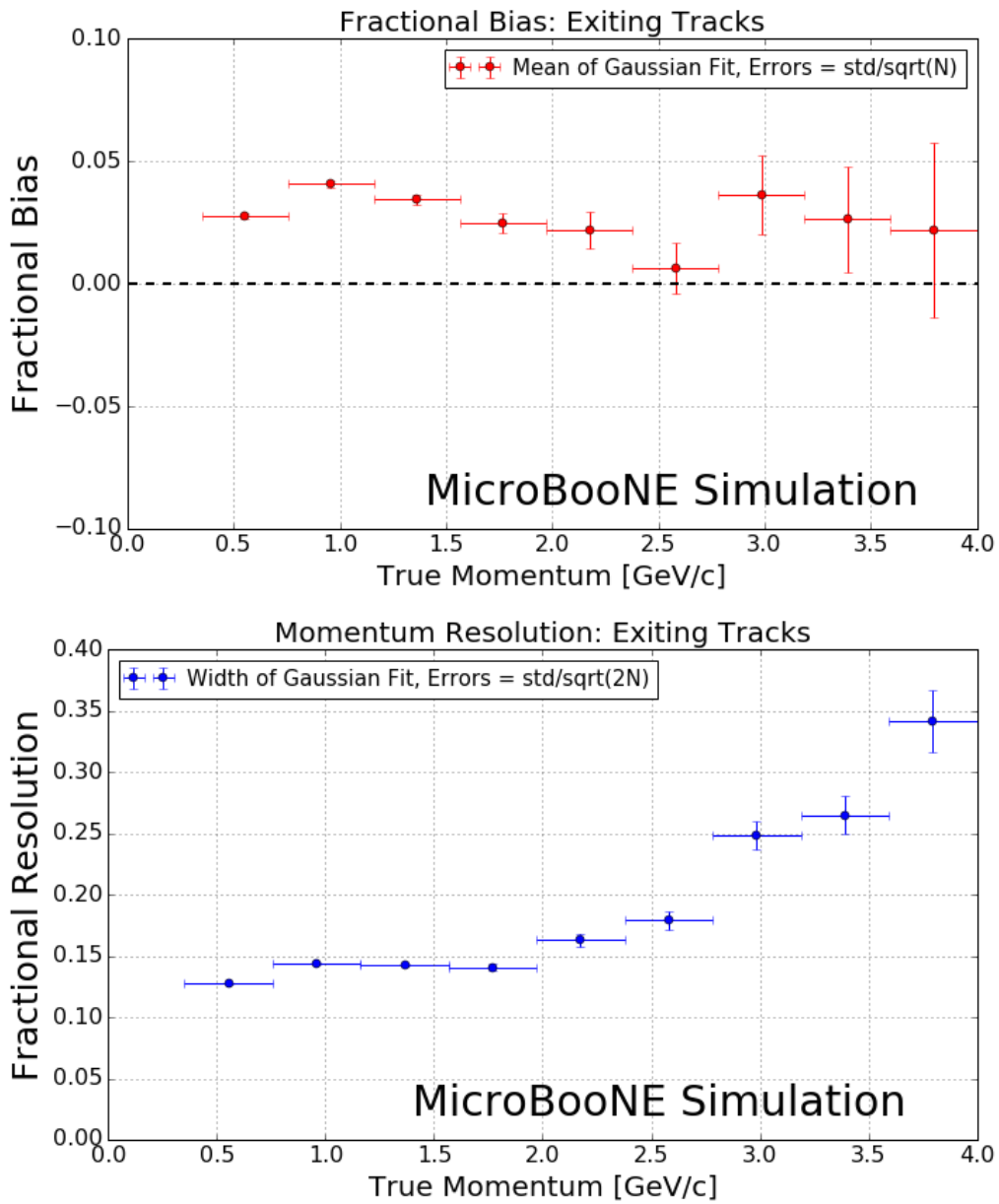


**Figure 12.** MCS momentum fractional bias (top) and resolution (bottom) as a function of true momentum from a sample of exiting reconstructed muon tracks.

344 **References**

- 345 [1] A. A. Aguilar-Arevalo *et al.* [MiniBooNE Collaboration], *Improved Search for  $\bar{\nu}_\mu \rightarrow \bar{\nu}_e$  Oscillations*  
346 *in the MiniBooNE Experiment*, Phys. Rev. Lett. **110**, 161801 (2013).  
347 [arXiv:1207.4809 [hep-ex], arXiv:1303.2588 [hep-ex]].
- 348 [2] C. Adams *et al.* [LArTPC Collaboration], *LAr1-ND: Testing Neutrino Anomalies with Multiple*  
349 *LArTPC Detectors at Fermilab*, arXiv:1309.7987 [physics.ins-det].
- 350 [3] F. Arneodo *et al.* [ICARUS Collaboration], *The ICARUS experiment: A Second generation proton*  
351 *decay experiment and neutrino observatory at the Gran Sasso Laboratory*, hep-ex/0103008.
- 352 [4] R. Acciarri *et al.* [DUNE Collaboration], *Long-Baseline Neutrino Facility (LBNF) and Deep*  
353 *Underground Neutrino Experiment (DUNE) : Volume 1: The LBNF and DUNE Projects*,  
354 arXiv:1601.05471 [physics.ins-det].
- 355 [5] R. Acciarri *et al.* [MicroBooNE Collaboration], *Design and Construction of the MicroBooNE*  
356 *Detector*, arXiv:1612.05824 [physics.ins-det].
- 357 [6] A. A. Aguilar-Arevalo *et al.* [MiniBooNE Collaboration], *The Neutrino Flux prediction at*  
358 *MiniBooNE*, Phys. Rev. D **79**, 072002 (2009)  
359 [arXiv:0806.1449 [hep-ex]].
- 360 [7] R. Acciarri *et al.* [MicroBooNE Collaboration], *Study of Space Charge Effects in MicroBooNE*,  
361 www-microboone.fnal.gov/publications/publicnotes/MICROBOONE-NOTE-1018-PUB.pdf.
- 362 [8] V. L. Highland, *Some Practical Remarks on Multiple Scattering*, Nucl. Instrum. Methods **129** (1975)  
363 104-120.
- 364 [9] G. R. Lynch and O. I. Dahl, Nucl. Instrum. Methods Section B (Beam Interactions with Materials  
365 and Atoms) **B58**, **6** (1991).
- 366 [10] K. Kodama *et al.* [DONUT Collaboration], *Observation of tau neutrino interactions*, Phys. Lett. B  
367 **504**, 218 (2001)  
368 [hep-ex/0012035].
- 369 [11] N. Agafonova *et al.* [OPERA Collaboration], *Momentum measurement by the Multiple Coulomb*  
370 *Scattering method in the OPERA lead emulsion target*, New J. Phys. **14**, 013026 (2012)  
371 [arXiv:1106.6211 [physics.ins-det]].
- 372 [12] G. Giacomelli [MACRO Collaboration], *Neutrino physics and astrophysics with the MACRO*  
373 *experiment at the Gran Sasso lab*, Braz. J. Phys. **33**, 211 (2003)  
374 [hep-ex/0210006].
- 375 [13] A. Ankowski *et al.* [ICARUS Collaboration], *Measurement of through-going particle momentum by*  
376 *means of multiple scattering with the ICARUS T600 TPC*, Eur. Phys. J. C **48**, 667 (2006)  
377 [hep-ex/0606006].
- 378 [14] M. Antonello *et al.*, *Muon momentum measurement in ICARUS-T600 LAr-TPC via multiple*  
379 *scattering in few-GeV range*, arXiv:1612.07715 [physics.ins-det].
- 380 [15] S. Agostinelli *et al.* Nucl. Instrum. Methods Phys. Res. **A506250-303** (2003)
- 381 [16] F. Cavanna *et al.* [LArIAT Collaboration], *LArIAT: Liquid Argon In A Testbeam*, arXiv:1406.5560  
382 [physics.ins-det].
- 383 [17] J. S. Marshall and M. A. Thomson, *The Pandora Software Development Kit for Pattern Recognition*,  
384 Eur. Phys. J. C **75**, no. 9, 439 (2015)  
385 [arXiv:1506.05348 [physics.data-an]].

- 386 [18] D. E. Groom, N. V. Mokhov and S. Striganov, *Muon Stopping Power and Range Tables: 10 MeV -*  
387 *100 TeV* Table 5, <http://pdg.lbl.gov/2012/AtomicNuclearProperties/adndt.pdf>
- 388 [19] H. Bichsel, D. E. Groom, S.R. Klein, *Passage of Particles Through Matter* PDG Chapter 27, Figure  
389 27.1 <http://pdg.lbl.gov/2005/reviews/passagerpp.pdf>
- 390 [20] Table 289: Muons in Liquid argon (Ar) [http://pdg.lbl.gov/2012/AtomicNuclearProperties/MUON\\_ELOSS\\_TABLES/muonloss\\_289.pdf](http://pdg.lbl.gov/2012/AtomicNuclearProperties/MUON_ELOSS_TABLES/muonloss_289.pdf)
- 391 [21] *Stopping Powers and Ranges for Protons and Alpha Particles*, ICRU Report No. 49 (1993); Tables  
393 and graphs of these data are available at <http://physics.nist.gov/PhysRefData/>
- 394 [22] D. Heck, J. Knapp, J. N. Capdevielle, G. Schatz, T. Throw, *CORSIKA: A Monte Carlo Code to*  
395 *Simulate Extensive Air Showers*, Forschungszentrum Karlsruhe Report FZKA 6019 (1998)